Published in final edited form as:
Biochemistry. 2013 December 10; 52(49): 8907–8915. doi:10.1021/bi401494f.

The formal reduction potential of 3,5-difluorotyrosine in a structured protein: Insight into multistep radical transfer

Kanchana R. Ravichandran[†], **Li Liang**[§], **JoAnne Stubbe**[†], and **Cecilia Tommos**[§,*]

[†]Department of Chemistry, Massachusetts Institute of Technology, 77 Massachusetts Avenue, Cambridge, Massachusetts 02139

[§]Graduate Group in Biochemistry & Molecular Biophysics and Department of Biochemistry & Biophysics, University of Pennsylvania, Philadelphia, Pennsylvania 19104, United States of America

Abstract

The reversible Y-O•/Y-OH redox properties of the α_3Y model protein enable access to the electrochemical and thermodynamic properties of 3,5-difluorotyrosine. The unnatural amino acid has been incorporated at position 32, the dedicated radical site in α_3Y, by *in vivo* nonsense codon suppression. Incorporation of 3,5-difluorotyrosine gives rise to very minor structural changes in the protein scaffold at pH below the apparent p*K* (8.0 ± 0.1) of the unnatural residue. Square-wave voltammetry on α_3(3,5)F_2Y provides an $E^{\circ\prime}$(Y-O•/Y-OH) of 1026 ± 4 mV *versus* the NHE (pH 5.70 ± 0.02) and shows that the fluoro-substitutions lower $E^{\circ\prime}$ by –30 ± 3 mV. These results illustrate the utility of combining the optimized α_3Y tyrosine radical system with *in vivo* nonsense codon suppression to obtain the formal reduction potential of an unnatural aromatic residue residing within a well-structured protein. It is further observed that the protein $E^{\circ\prime}$values differ significantly from peak potentials derived from irreversible voltammograms of the corresponding aqueous species. This is significant since solution potentials have been the main thermodynamic data available for amino-acid radicals. These findings are discussed relative to recent mechanistic studies on the multistep radical-transfer process in *E. coli* ribonucleotide reductase site-specifically labeled with unnatural tyrosine residues.

Tyrosine serves as a one-electron redox cofactor in catalytic and multistep electron-transfer reactions (1-5). It has been challenging to obtain precise and accurate thermodynamic information for this high-potential protein redox species. Electrochemical characterization of the natural systems has not been feasible due to their size, complexity and sensitivity to oxidative damage. Mechanistic studies on redox proteins employing tyrosine radical (Y•) cofactors must thus partly rely on model systems to provide insights to the thermodynamics involved. Reduction potentials (*E* values) of aqueous Y and various analogues have been

[*]**Corresponding Author** All correspondence should be addressed to: Dr. Cecilia Tommos, 905 Stellar-Chance Laboratories, Department of Biochemistry & Biophysics, University of Pennsylvania, 422 Curie Blvd, Philadelphia, PA 19104-6059. Telephone: 215-746-2444; Facsimile: 215-573-7290; tommos@mail.med.upenn.edu.

Supporting Information. Materials and Methods; α_3(3,5)F_2Y protein expression analysis (Fig. S1); HPLC and MALDI-TOF evaluation of purified α_3(3,5)F_2Y (Fig. S2); pK_{app} fitting analysis (Fig. S3); chemical denaturation plots of α_3(3,5)F_2Y and α_3Y at pH 5.0 and 5.5 (Fig. S4); α_3(3,5)F_2Y I_{net} as a function of E_{SW} (Fig S5). This material is available free of charge via the internet at http://pubs.acs.org.

obtained by pulse radiolysis and voltammetry methods (6-11). Considerable uncertainty is associated with the reported values. This is in part due to varying experimental conditions, comparison of neutral and zwitterionic amino acids, and complicating issues such as solvent oxidation and the perturbation of solute/working electrode interactions. The most significant uncertainty, however, arises from the reactivity of the radical species themselves. Tyrosine radicals generated in solution will rapidly dimerize (~ 5×10^8 M^{-1} s^{-1}; 12-16) and give rise to quasi/irreversible voltammograms (17, 18). Peak potentials (E_{peak}) derived from such data reflect the electrode process (electrode driven oxidation-reduction of Y) as well as the thermodynamics and kinetics of the coupled side reactions (chemical reduction of Y•). The observed potentials may thus differ by 10s even 100s of millivolts from the formal (true) reduction potential ($E^{\circ\prime}$) of the Y redox system. Comparison between aqueous solution and protein Y redox chemistry is further complicated by the significant differences in the fundamental properties of these two media (19, 20).

The α_3X family of well-structured proteins was developed to address these concerns (10, 21). This model protein system yields thermodynamic information that is uncompromised by electrochemical irreversibility and radical side reactions (22-24). The α_3X proteins are based on a common *de novo* designed three.helix bundle scaffold: Scheme 1 displays helical and loop regions in bold and italic, respectively. The N-terminal GS of the 67-residue sequence form part of a thrombin cleavage site and are labeled as –2 and –1 to keep the amino-acid numbering consistent between the chemically synthesized (10) and recombinantly expressed (25, 26) α_3X proteins. The buried redox site (position 32 in the middle of the central helix) is occupied by a tryptophan (to form the α_3W protein), a tyrosine (α_3Y), or a cysteine (α_3C). C32 has been used to covalently attach phenol (24, 26) and quinone (27) molecules to the protein scaffold. All of the α_3X proteins display very similar structural characteristics. They are stable and well-structured from pH ~4 to 10. Their single aromatic residue (W, Y, phenol or quinone) gives rise to UV-Vis, fluorescence and NMR spectra that are highly sensitive to the microenvironment of the redox site. Protein voltammetry has shown that the α_3X system displays unique electrochemical properties. The protein scaffold is redox inert to at least +1.3 V *vs.* NHE (22, 24, 26). The system becomes redox active when a W (10), Y (22, 23), phenol (24, 26) or quinone (27) is introduced at position 32. Fully reversible voltammograms and $E^{\circ\prime}$ values have thus far been reported for the Y and phenol-containing α_3X proteins (22, 24).

In this study we use the α_3X system in combination with the *in vivo* nonsense codon suppression method (28) and square-wave voltammetry (SWV; 17, 29, 30) to determine $E^{\circ\prime}$ for a protein 3,5-difluorotyrosine (3,5-F_2Y) residue. We report $\Delta E^{\circ\prime}$ between 3,5-F_2Y and Y residues obtained at highly comparable experimental conditions. The results are compared to published solution potentials and discussed relative to recent mechanistic studies on *E. coli* class Ia ribonucleotide reductase (RNR) site-specifically labeled with unnatural Y residues in an effort to understand the thermodynamic and kinetic landscape of the proton-coupled electron transfer (PCET) pathway in this system (28, 31, 32).

MATERIALS AND METHODS

Purification of tyrosine phenol lyase (TPL)

E. coli strain SVS370 harboring the plasmid pTZTPL was obtained as a gift from Dr. Robert Phillips (University of Georgia). pTZTPL encodes TPL under a constitutive promoter and the protein was expressed and purified (33, 34) using a slightly modified procedure. The elution fractions from the octyl-sepharose column were assayed using a coupled spectrophotometric assay where a small volume of the fraction was added to an assay mixture containing 2 mM L-tyrosine, 5 mM β-mercaptoethanol, 50 μM pyridoxyl-5′-phosphate, 0.3 mg/mL lactate dehydrogenase (*L. leichmannii* from Sigma-Aldrich) and 0.2 mM NADH in 50 mM potassium phosphate pH 8.0. The reaction was monitored at 340 nm for the disappearance of NADH. Fractions containing considerable activity were pooled and concentrated in an Amicon ultrafiltration cell with a YM 10 membrane and the protein was used with no additional purification steps. One unit (U) of activity is defined as 1 μmol product/min. A total of 62 U/g cell paste was obtained, in excellent agreement with the previously reported yield (33).

Enzymatic synthesis of 3,5-difluorotyrosine (3,5-F_2Y)

TPL was used to enzymatically synthesize 3,5-F_2Y from 2,6-difluorophenol (the numbering of the aromatic ring changes as the OH carbon is position 1 in the phenol and position 4 in the amino acid). Briefly, a one or two liter reaction mixture containing 10 mM 2,6-difluorophenol, 30 mM ammonium acetate pH 8.0, 60 mM sodium pyruvate, 5 mM β-mercaptoethanol, 40 μM pyridoxyl-5′-phosphate and 30 U of TPL at room temperature was stirred in the dark for a total of four days. The mixture was supplied with additional TPL, β-mercaptoethanol and pyridoxyl-5′-phosphate every other day. Once the reaction was complete (as assessed by TLC), the mixture was worked up as described in Ref. 34. The yield is typically > 85% for 3,5-F_2Y and the final product was characterized by ^{1}H and ^{19}F NMR spectroscopy (11, 35).

Construction of α_3TAG32 by site-directed mutagenesis

The amber stop codon (TAG) was introduced at position 32 of α_3Y using a modified pET32b-α_3Y plasmid (22, 25) as template and forward primer 5’- GGC GGC CGT ATT GAA GAA CTG AAA AAA AAA TAG GAA GAA CTG AAA AAA AAA ATT GAA GAA CTG GGC GGC GGC-3’ and reverse primer 5’- GCC GCC GCC CAG TTC TTC AAT TTT TTT TTT CAG TTC TTC CTA TTT TTT TTT CAG TTC TTC AAT ACG GCC GCC-3’. The mutation was performed using the Stratagene QuikChange kit and confirmed by sequencing at the MIT Biopolymers Laboratory.

Expression of α_3(3,5)F_2Y

pET32b-α_3TAG32 was co-transformed with a plasmid (pEVOL-F_nY-RS) encoding the fluorotyrosine tRNA and aminoacyl-tRNA synthetase (F_nY-RS) genes (28) into BL21(DE3) competent cells and grown on media containing ampicillin (100 μg/mL) and chloramphenicol (35 μg/mL) at 37° C. Unnatural amino-acid concentration and protein expression were optimized on a small-scale resulting in the following protocol: 40 mL LB

pre-cultures were started from single colonies, grown for ~ 16 h, and used to inoculate (50-fold dilution) 1 L 2x YT cultures containing 2.0 mM 3,5-F_2Y. 3,5-F_2Y additions were made from stock solutions freshly prepared in water, NaOH solubilized and sterile filtered. The expression of F_nY-RS was induced at an OD_{600} of 0.2-0.3 (L-arabinose, final concentration 0.05% (w/v)). The expression of α_3(3,5)F_2Y was induced at an OD_{600} of 0.5 (IPTG , final concentration 1mM). Growth was continued for an additional 4 h and the cells were harvested by centrifugation (5000 × g, 15 min, 4° C). Protein expression was monitored by SDS-PAGE. No toxicity was seen due to the unnatural amino acid. A typical yield of 0.5 g cell paste/100 mL and 2.5 g cell paste/L media was obtained for the 0.1 and 1 L cultures, respectively.

Purification of α_3(3,5)F_2Y

Cell paste (~ 5-10 g) was resuspended (5 mL/g paste) in buffer A (20 mM Tris-HCl, 500 mM NaCl, 5 mM imidazole, pH 7.9), treated with lysozyme (300 μg/mL, 30 min, 30° C) and lysed by sonication. The lysate was clarified by centrifugation (12000 × g, 20 min, 4° C), passed over a nickel column (10 mL His•bind resin, EMD Millipore) equilibrated with buffer A, and the thioredoxin fusions eluted with a linear 0–40% buffer B (20 mM Tris-HCl, 500 mM NaCl, 1M imidazole, pH 7.9) gradient over 40 min (flow rate 1.5 mL/min). Fractions containing the thioredoxin fusions were identified by SDS-PAGE. Thrombin (T6634; Sigma-Aldrich) was added to the pooled fusion-protein fractions (thrombin/protein ratio 1:2000 (w/w)) and the resulting mixture dialyzed against 20 mM Tris-HCl, 500 mM NaCl, 2.5 mM $CaCl_2$, pH 8.0 at RT for >16 h. The thrombin digestion produces three major products: His- tagged thioredoxin, the truncated α_3(residue 1–31) peptide (MW 3579 Da) and the full-length α_3(3,5)F_2Y protein (MW 7557 Da). A major fraction of the truncated α_3(residue 1–31) product was removed during the overnight dialysis step (Spectra/Por tubing MWCO 3500 Da). The digestion/dialysis mixture (~ 30 mL) was passed over a nickel column (10 mL His•bind resin equilibrated with buffer A) to remove the His-tagged thioredoxin and any remaining undigested fusion products. α_3(3,5)F_2Y (sample injection volume 5-10 mL) was isolated by reversed-phase HPLC (218TP C18 column, particle size 10 μm, column size 10 × 250 mm; Grace/VYDAC) using an linear water/acetonitrile/0.1% (w/v) trifluoroacetic acid gradient (30-60% acetonitrile over 45 min, flow rate 5 mL/min), and stored as lyophilized powder. The protein purification steps were monitored by SDS-PAGE. Purity was evaluated by reversed-phase HPLC (218TP C18 column, particle size 5 μm, column size 4.6 × 250 mm; Grace/VYDAC) using a linear water/acetonitrile/0.1% (w/v) trifluoroacetic acid gradient (20-70% acetonitrile over 50 min, flow rate 1 mL/min). Molecular weights were verified by matrix-assisted desorption/ionization-time of flight (MALDI-TOF) mass spectrometry using a Bruker Microflex 3.1. An average yield of ~3 mg pure α_3(3,5)F_2Y/L culture was observed.

Absorption spectroscopy

Absorption spectra were recorded on a Varian Cary 50 Bio UV-Vis spectrometer at RT. Protein concentrations were determined by the Bradford protein assay (Bio-Rad) with standard curves prepared using either bovine serum albumin (for thioredoxin fusion samples) or α_3W (10) (for α_3Y and α_3(3,5)F_2Y protein-characterization samples). An ε_{280} of 5690 M^{-1} cm^{-1} was used for α_3W (10, 36, 37) when preparing the standard curves. The

apparent tyrosinate/tyrosine pK_a (pK_{app}) of (3,5)F_2Y_{32} was measured by dissolving lyophilized α_3(3,5)F_2Y in 3.0 mL 20 mM sodium acetate, 20 mM potassium phosphate, 20 mM sodium borate (APB buffer), pH 12 to give an absorption of 0.2 at 277 nm (10 mm path). The protein stock solution was added to 20 mM APB buffer generating two samples with pH ~ 5 and 12, respectively. The pH was pre-adjusted in the APB buffer samples to generate the final pH upon addition of the protein stock. The protein dilution was 2-fold providing a final 277 nm absorption of 0.1 (10 mm path; pH 12). Equal-volume (1.6 mL) titration was performed manually by removing a 100-400 μL portion from the cuvette containing the high-pH sample and then adding the same amount of low-pH sample per pH adjustment. The pK_{app} was obtained by fitting the pH-induced increase in the (3,5)F_2Y_{32}-O^- absorption to a single pK_a.

Circular dichroism (CD) spectroscopy

CD data were collected on an Aviv 202 CD spectrometer at 25° C. The instrument was equipped with an automated titration system. For the α-helical measurements, CD spectra were collected from α_3W, α_3Y and α_3(3,5)F_2Y dissolved in 20 mM sodium acetate, pH 5.6. Protein concentrations were determined by the Bradford assay and using α_3W as the standard. pH titrations were performed by dissolving lyophilized protein in 20 mM APB buffer, pH 4.8 to a 235 nm ellipticity of ~–175 mdegrees (10 mm path). The protein stock solution was added to 20 mM APB buffer generating two samples with pH ~ 4 and 10, respectively. The pH was pre-adjusted in the APB buffer samples to generate the final pH upon addition of the protein stock. The protein dilution was 4-fold generating a final 222 nm ellipticity ~–150 mdegrees (10 mm path; pH 4). Equal-volume (2.5 mL) titration was performed manually by removing a 40-1000 μL portion from the cuvette containing the high-pH sample and then adding the same amount of low-pH sample per pH adjustment. Protein stability measurements were conducted by dissolving lyophilized protein in 20 mM sodium acetate, 20 mM potassium phosphate (AP buffer), pH 5.0 or 5.5 buffer to a 230 nm ellipticity of –75 to –140 mdegrees (1 mm path). The protein stock solution was added to 20 mM AP buffer containing 0 and 9.5 M urea, respectively. The pH was 5.0 or 5.5 in the protein/AP buffer and protein/AP buffer/urea solutions. The protein dilution was 18-fold generating a final 222 nm ellipticity in the –110 to – 210 mdegrees range (10 mm path) at zero molar denaturant. The urea denaturation experiments were performed by automated equal-volume (2.0 mL) titration controlled from the Aviv software. Global stability values were determined by fitting the denaturation curves as described in Ref. 38.

Square-wave voltammetry (SWV)

Voltammetry measurements (17, 29, 30) were performed using an Autolab PGSTAT12 potentiostat equipped with a temperature-controlled, Faraday-cage protected three-electrode micro-cell (Princeton Applied Research). The Ag/AgCl reference electrode and the platinum wire counter electrode (Advanced Measurements Inc.) were stored dry and prepared by filling the former with a 3M KCl/saturated AgCl solution and the latter with sample buffer. All measurements were carried out using a 3 mm diameter pyrolytic graphite edge (PGE) working electrode (Bio-Logic, USA). The electrode surface was activated between measurements by manually polishing its surface for 60 s in a 1.0 μm diamond/water slurry on a diamond polishing pad (Bio-Logic, USA) followed by 60 s in a 0.05 μm alumina/water

slurry on a microcloth pad (Bioanalytical systems Inc.). The electrode was rinsed with an excess of methanol followed by milli-Q water directed against the surface of the electrode. Measurements were performed immediately following the polishing procedures. Solution resistance was compensated for by using the positive feed-back iR compensation function of the Autolab system. Potentials are given *versus* the normal hydrogen electrode (NHE). All samples were prepared from ultra-pure chemicals and the measurements performed under an argon atmosphere. Preparation of the voltammetry protein samples is described in the main text. Protein concentration series were obtained by stepwise dilution of the protein samples in the electrochemical cell while keeping the sample volume constant at 2.5 mL. The pH was monitored directly in the electrochemical cell using a pH microelectrode (Microelectrodes Inc.) connected to a SevenMulti pH meter (Mettler Toledo). The pH electrode was disconnected from the pH meter during the active measurements to avoid the risk of introducing electric noise. Data processing and analyses were performed using the Autolab GPES software and PeakFit (Systat Software Inc.).

RESULTS

$\alpha_3(3,5)F_2Y$ expression and purification

3,5-difluorotyrosine was synthesized enzymatically (33, 34) as described in the Materials and Methods section. The amber stop codon (TAG) was introduced in place of the codon for residue 32 (Scheme 1) in a modified pET32b plasmid used for expression of the α_3X proteins (22, 25). The α_3TAG variant was co-expressed with an evolved polyspecific fluorotyrosine aminoacyl-tRNA synthetase (28) in *E. coli* BL21(DE3) cells. Protein expression was initially evaluated in 100 mL growth cultures by SDS-PAGE and mass spectrometry. Optimal expression was observed with 2.0 mM 3,5-F_2Y in 2x YT media (see Fig. S1 in the Supporting Information). The growth cultures were scaled to 1 L to generate sufficient material for protein characterization and voltammetry studies. Protein expression and purification protocols are described in detail in Materials and Methods. The purity of the $\alpha_3(3,5)F_2Y$ preparations was evaluated by reversed-phase HPLC (Fig. S2A) and the correct protein molecular weight was verified by mass spectrometry (Fig. S2B). The average yield of pure $\alpha_3(3,5)F_2Y$ was ~3 mg/L culture, which represents a suppression efficiency of only ~10%. Efforts to improve the suppression efficiency are in progress.

Protein characterization

The aims of this study are to determine (i) the electrochemical reversibility of $\alpha_3(3,5)F_2Y$, (ii) $E^{\circ\prime}$ of $(3,5)F_2Y_{32}$, and (iii) $\Delta E^{\circ\prime}$ between $(3,5)F_2Y_{32}$ and Y_{32} when recorded at near identical conditions. Initially we compared the structural properties of α_3Y and $\alpha_3(3,5)F_2Y$. α_3Y is highly helical and well-structured from pH 4.5 to 10 (10, 22). The apparent Y-O^-/Y-OH pK_a (pK_{app}) of Y_{32} is 11.3 ± 0.1 (Table 1). Exchanging Y_{32} to $(3,5)F_2Y_{32}$ was not expected to significantly perturb the protein scaffold (39, 40) at pH conditions where the buried phenol side chain is uncharged. Experiments were carried out to determine a suitable pH range for the SWV analysis, i.e., where $(3,5)F_2Y_{32}$ remains protonated and the structural properties of $\alpha_3(3,5)F_2Y$ closely resemble those of α_3Y.

Figure 1A displays absorption spectra of $\alpha_3(3,5)F_2Y$ collected over a pH 5.7 (grey) to 10.4 (purple) range. The $(3,5)F_2Y_{32}$-O^-/$(3,5)F_2Y_{32}$-OH transition titrates with a pK_{app} of 8.0 ± 0.1 (see Fig. S3 for details). The protein environment increases the pK_{app} by ~1 unit relative to aqueous 3,5-F_2Y (pK_a 7.0 ± 0.2; Table 1; 11, 35). The weak and blue shifted absorbance of aqueous 3,5-F_2Y-OH (ε_{263} 560 M^{-1} cm^{-1}) relative to unmodified Y-OH (ε_{275} 1490 M^{-1} cm^{-1}; Table 1) was expected to translate into a rather poorly defined absorption spectrum of $\alpha_3(3,5)F_2Y$. The blue shift increases the spectral overlap between the absorption of the aromatic side chain and the large absorption of the protein backbone (λ_{max} 190-220 nm) making $\alpha_3(3,5)F_2Y$ concentration measurements based on UV absorbance unreliable. Thus, the Bradford method was used to determine protein concentrations with standard curves prepared from α_3W. ε_{277} of 1500 ± 80 (pH 5.4) and ε_{294} of 2430 ± 130 (pH 13.4) M^{-1} cm^{-1} were obtained for Y_{32}-OH and Y_{32}-O^- in α_3Y, respectively. The ε_{277} value is consistent with the average ε_{280} of 1490 M^{-1} cm^{-1} typically used for protein Y-OH residues (36, 37) and close to the ε_{max} values of aqueous Y-OH (Table 1; 11). We conclude that the Bradford assay determines the α_3X protein concentration with good accuracy.

CD spectroscopy was used to measure the absolute α-helical content, the pH sensitivity of this parameter, and the global stability of $\alpha_3(3,5)F_2Y$ relative to α_3Y (Table 1). Figure 1B displays far-UV CD spectra of $\alpha_3(3,5)F_2Y$ (blue) and α_3Y (red) collected at pH 5.6. The reference spectrum of the structurally characterized α_3W protein (green; 10, 25) is also shown. The protein concentration in the CD samples was determined by the Bradford method. The CD spectral line shapes are essentially identical and display the characteristic 208/222 nm double minima of a predominantly α-helical protein. The 222 nm mean residue molar ellipticity ($[\Theta]_{222}$) reflects the α-helical content, which was estimated to ~75-80% for $\alpha_3(3,5)F_2Y$ and α_3Y at pH 5.6 (Table 1). This translates into 50 ± 1 residues with helical ψ and ϕ backbone angles in $\alpha_3(3,5)F_2Y$ and α_3Y. This degree of helicity has consistently been observed for structurally characterized α_3X proteins (α_3W PDB ID 1LQ7 (25); 2-mercaptophenol-α_3C 2LXY (24)). Figure 1C displays $[\Theta]_{222}$ and the corresponding % helix of $\alpha_3(3,5)F_2Y$ as a function of pH. The α-helical content of $\alpha_3(3,5)F_2Y$ decreases by only 2% from pH 4.7 to 6.7 and by 6% from pH 6.7 to 10. These small pH-induced changes in helical content are likely to be driven by the deprotonation of $(3,5)F_2Y_{32}$. The global stability of $\alpha_3(3,5)F_2Y$ and α_3Y was thus compared at acidic pH > two pH units below the pK_{app} of $(3,5)F_2Y_{32}$ (Fig. S4). The stability of the two proteins was found to be identical at pH 5.0 and differ by only 0.2 kcal mol^{-1} at pH 5.5 (Table 1). The SWV analysis described below was conducted at low pH (5.6 ± 0.1) where the structural properties of $\alpha_3(3,5)F_2Y$ and α_3Y are very similar and their phenols are protonated.

Preparation of SWV samples

The protein concentration is a key parameter to control when investigating the protein/working electrode interactions and optimizing the Faradaic response (23, 24). The high α-helical content of $\alpha_3(3,5)F_2Y$ makes CD spectroscopy a precise method to determine the protein concentration in a highly reproducible manner. Voltammetry samples were thus prepared by dissolving lyophilized protein in buffer until an appropriate θ_{222} and the protein concentration was calculated from the determined $[\Theta]_{222}$ value (see Fig. 1 legend and Table

1). The supporting electrolyte, KCl, was added to the samples after the CD measurements to avoid UV absorption of the chloride ion.

SWV analysis of $\alpha_3(3,5)F_2Y$

SWV voltammetry was conducted using a PGE working electrode. In SWV, the base potential (E_{step}) is changed incrementally in a series of forward and reverse pulses (17, 29, 30). The pulse height and length are set by the SW amplitude (E_{SW}) and frequency (f), respectively. The current is sampled at the end of each alternating pulse and traced out as a function of E_{step}. The pulse train generates a forward (I_{for}), a reverse (I_{rev}), and a net ($I_{net} = I_{for} - I_{rev}$) voltammogram. Previous studies using the PGE electrode have shown that ~20–100 μM α_3X in 20 mM APB buffer and 60–140 mM KCl yields Y and phenol voltammograms with optimal S/N at both acidic (5.5) and alkaline (8.5) pH (23, 24). At these conditions, the system is governed by diffusion-controlled kinetics, the protein does not unfold on the electrode surface, and the observed potential is independent of functional groups present at the electrode surface. The $\alpha_3(3,5)F_2Y$ SWV measurements were consequently conducted using 20 mM APB and 75 mM KCl. Overall, $\alpha_3(3,5)F_2Y$ displays electrochemical properties very similar to those of α_3Y (23). The Faradaic response is consistent with diffusion-controlled kinetics (Fig. S5) and benign $\alpha_3(3,5)F_2Y$/working electrode interactions (Figs. 2A and B). Figure 2C shows the change in the peak potential of the forward (I_{for}), reverse (I_{rev}) and net (I_{net}) currents as a function of the SW frequency. Background-corrected voltammograms from this data series are shown in Figs. 2D-F. E_{for}, E_{rev} and E_{net} level off and come together as the SW frequency increases. This is consistent with a redox system that is shifting from the upper quasi-reversible region towards the fully reversible region as the SW frequency increases (29, 30). E_{net} of 1026 ± 3 mV, E_{for} of 1021 ± 3 mV, and E_{rev} of 1032 ± 2 mV are observed for the 270-540 Hz range at pH 5.70 ± 0.02. The observed frequency insensitivity and small separation in peak maxima mean that E_{net} closely approximates $E^{\circ\prime}$ (i.e. within a few mV; 23, 24, 30). With a pK_{app} of 8.0, we calculate $E^{\circ\prime}$(pH 7.0) to be 952 mV (Table 1). Comparing these results with the earlier reported α_3Y SWV study (23), provides an $E^{\circ\prime}$ between Y_{32} and $(3,5)F_2Y_{32}$ of –28-33 mV. This result was reproduced in a control experiment where $\alpha_3(3,5)F_2Y$ and α_3Y SW voltammograms were collected at identical experimental conditions, using the same electrode setup (Fig. 3, ΔE_{net} –30 ± 3 mV). We conclude that $E^{\circ\prime}$ of the Y32-O•/Y32-OH redox pair is lowered by 30 ± 3 mV upon fluoro-substitution at ring positions 3 and 5 (carbon atoms next to the phenol oxygen). We further note that the difference between E_{peak} of aqueous Y and $E^{\circ\prime}$ of α_3Y is –150 mV, with the protein being the more oxidizing system (Table 1).

DISCUSSION

Measuring tyrosine reduction potentials

There are three basic properties associated with tyrosine that make electrochemical characterization a major challenge. The measurements must be carried out at highly oxidizing conditions (~ 1.0 ± 0.3 V *vs.* NHE), the Y• state is reactive (e.g. 12-16), and both the reduced (ε_{280} 1490 M^{-1} cm^{-1}; 36, 37) and oxidized (ε_{408} of 2750 M^{-1} cm^{-1}; 41) states have weak extinction coefficients. The combination of these three properties rule out redox

titration as a viable method to study the thermodynamics of Y redox cofactors. This is significant since redox titration, using either chemical titrants and a redox cuvette or a potentiostat-controlled spectroelectrochemical cell, is the most common approach to measure reduction potentials of protein redox cofactors. The two former properties also make voltammetry a challenge. Measurements performed in the + 1.0 V range will generate background currents arising from the working electrode and from the water solvent itself. These background currents will compromise data analysis unless the Faradaic current reflecting the Y redox cofactor is prominent. Moreover, uncontrolled oxidation of surface residues and general oxidative damage to the host protein are likely events. In addition to these concerns are the inherent issues associated with protein voltammetry, i.e., to identify conditions for which the folded protein exhibits direct and reversible electron transfer between the working electrode and the redox site of interest (42-44). These are the main reasons that a direct voltammetry approach on a complex radical enzyme such as *E. coli* RNR is not practical or even possible.

The α_3X system was developed to address these experimental barriers and allow rigorous electrochemical characterization of aromatic amino acids buried within a structured protein. In three recent studies (22-24), we have demonstrated that pulsed voltammetry methods (differential pulse voltammetry and SWV) generate reversible Y and phenol protein voltammograms of high quality. Control studies have shown that the characteristics of the α_3X voltammograms are highly reproducible and that they uniquely reflect the aromatic residue at position 32 and its local environment. The more commonly used method of cyclic voltammetry (17) generates a poor Faradaic response from the α_3X proteins (22) and this method was deemed too insensitive for this system. We note that the potential range probed in this study is very oxidizing for a protein system with measured E_{net} values well above +1.0 V. The high quality of the presented voltammograms is the result of combining the sensitivity provided by the pulsed SWV method (due to effective elimination of capacitative background currents) with carefully optimized protein/PGE working electrode conditions. The latter include electrode polishing procedures (described in the Materials and Methods sections), the sample composition (optimized for the α_3X/PGE system in Refs. 23 and 24), and the protein concentration (Fig. 2A). Importantly, the electrochemical reversibility observed for the α_3X proteins reflects the long halftimes (> 100s of ms) of the radicals generated in this system (23, 24). Thus, the protein environment efficiently blocks the deleterious Y• side reactions that typically compromise electrochemical characterization of the solvated species.

In this study the optimized α_3X radical system was combined with *in vivo* nonsense codon suppression (28) to measure $E^{\circ\prime}$ of a protein 3,5-F_2Y residue. The use of unnatural amino acids to study protein electron-transfer (ET) and proton coupled electron-transfer (PCET) processes involving Y redox sites has emerged as an informative experimental approach (31, 45, 46). The Y analogues provide a means to introduce major changes in the pK_a of the reduced state and in the $E^{\circ\prime}$ values of the Y-O•/Y-OH and Y-O•/Y-O^- redox couples. The pK_a of the oxidized state (–2 for aqueous Y-OH•+; 47) is predicted to be non-accessible within the structural and catalytic pH ranges of proteins. Residue 32 resides in a structured, solvent-protected and low dielectric site typical of natural Y redox cofactors. The α_3X

radical system will be used to generate a consistent set of $\Delta E^{\circ\prime}$ values to provide a guide for interpreting mutation-induced changes in the free-energy profile of native ET/PCET chains involving aromatic amino-acid redox site(s). The availability of protein $E^{\circ\prime}$ values removes the uncertainty associated with using solution potentials to interpret protein redox events. Table 1 shows that there are considerable differences in protein potentials obtained under reversible conditions relative to solution potentials obtained under irreversible conditions. We find a difference between $\Delta E^{\circ\prime}$ (protein Y_{32} and 3,5-F_2Y_{32}, –30 ± 3 mV) and ΔE_{peak} (aqueous Y and 3,5-F_2Y, –60 mV) of 30 mV (Table 1). This difference most certainly arises from the irreversible characteristics of the small-molecule measurements. We also found that the absolute values of $E^{\circ\prime}$ (protein Y_{32} and 3,5-F_2Y_{32}) *vs.* E_{peak} (aqueous Y and 3,5-F_2Y) is rather large (–150-180 mV). This observation suggests that the influence by the protein matrix on the absolute potentials of radical cofactors may be substantial. We conclude that site-specific incorporation of an unnatural amino acid into the electrochemically reversible α_3X redox system is a feasible and informative approach. It will be expanded to include other Y analogues in future studies, as described in more detail below.

Using the α_3X system as a guide to interpret mechanistic studies of E. coli RNR

RNRs catalyze the formation of deoxynucleotides (dNDPs) from their corresponding nucleotides (1, 31). *E. coli* class Ia RNR is composed of two homodimeric subunits, α2 and β2. A stable diferric-Y_{122}• cofactor in β2 generates a transient cysteine radical (C_{439}•) in the active site of α2 located 35 Å away. The reversible long range radical-transfer process, triggered by substrate and effector binding to α2, is proposed to involve multiple PCET steps via a conserved pathway ($Y_{122} \Leftrightarrow [W_{48}] \Leftrightarrow Y_{356}$ in β2 to $Y_{731} \Leftrightarrow Y_{730} \Leftrightarrow C_{439}$ in α2; 31). We have recently described the site-specific insertion of 3-nitrotyrosine (NO_2Y) in place of Y_{122} inβ2 (48). The diferric-NO_2Y_{122}• cofactor was generated and studies with α2, substrate (CDP) and effector (ATP) allowed the first observation of a transient, kinetically competent Y• on pathway by electron paramagnetic resonance (EPR) spectroscopy (48). Pulsed electron-electron double resonance (PELDOR) spectroscopy was used to establish the primary location of the new radical as Y_{356}•-β2 and suggested the formation of a small percentage of radical at either Y_{731} or Y_{730} in α2. To probe this further, the reaction of diferric-NO_2Y_{122}•-β2 with (3,5)F_2Y_{731}-α2 (or (3,5)F_2Y_{730}-α2), CDP and ATP was performed. Analysis of the reactions by X-band EPR spectroscopy demonstrated an equilibrium between Y_{356}• in β2 and (3,5)F_2Y_{731}• or (3,5)F_2Y_{730}• in α2 with 85-90% of the spin localized at Y_{356} and 15-10% distributed over F_2Y_{731}/F_2Y_{730} (32). To extrapolate the equilibrium observed with 3,5-F_2Y to Y, the native pathway residue, requires a knowledge of $E^{\circ\prime}$ values for 3,5-F_2Y and Y. To date only solution E_{peak} values derived from irreversible voltammograms have been available for the fluorotyrosines (11, 31). The SWV measurements performed on α_3Y and α_3(3,5)F_2Y provide the first $E^{\circ\prime}$ values representing the radical species in a well-defined protein environment. The small $\Delta E^{\circ\prime}$ of –30 ± 3 mV between Y_{32} and 3,5-F_2Y_{32} suggests that a thermodynamic landscape, formed by three transient tyrosyl radicals (Y_{356}, Y_{731}, Y_{730}) of similar energy with one (Y_{356}) being most prevalent, is a reasonable depiction of nature's design within this part of the pathway.

Future perspectives

We have shown that formal reduction potentials representing a reversible Y-O•/Y-OH redox system can be obtained for α_3Y (23) and α_3(3,5)F_2Y (this work). Future studies will involve the incorporation of other modified amino acids at position 32 in the α_3X scaffold to obtain a consistent set of $E^{\circ\prime}$ values from Y and modified Y residues. To determine $E^{\circ\prime}$ of 3-aminotyrosine (NH_2Y) and 2,3,5-trifluorotyrosine (2,3,5F_3Y) incorporated into the α_3X protein is of particular interest. In the former case, studies with NH_2Y in place of Y_{356}, Y_{731} and Y_{730} show an active pathway and that dNDPs can be produced (49). This is an interesting observation since the solution potential of NH_2Y (9) suggests that this species may act as a radical sink shutting down the pathway, as observed in experiments on 3,4-dihyroxyphenylalanine (DOPA)-labeled Y_{356}-β2 (50). Obtaining a solid protein $\Delta E^{\circ\prime}$ value for NH_2Y_{32} *vs.* Y_{32} would be valuable for interpreting the characteristics of the NH_2Y-labeled RNR systems (see Ref. 31 for more details). In the latter case, experiments are in progress in an effort to measure the thermodynamics between Y_{122} and Y_{356} in β2. Toward that goal, diferric-F_nY_{122}• (*n* = 2 or 3)-β2s have been successfully generated and the reactions of (3,5)F_2Y_{122}•-β2 and (2,3,5)F_3Y_{122}•-β2 with α2, CDP and ATP have been analyzed by EPR spectroscopy (28, 31). These studies reveal that only (2,3,5)F_3Y_{122}• is capable of generating a new pathway radical that is postulated to be Y_{356}•. Detailed investigations are ongoing with F_nY-β2s and wt-α2 and Y_{731}F-α2 to establish if there is an equilibrium between Y_{356}• and F_nY_{122}. Thus, protein $E^{\circ\prime}$values of (2,3,5)F_3Y and other F_nY residues relative to Y may also play an important role in defining the thermodynamic landscape within this part of the pathway. Finally, work to complement the α_3X protein $E^{\circ\prime}$ data series with α_3W is also in progress. Tryptophan is an important protein redox cofactor observed in a number of enzymes (e.g. 51-53), proposed to participate in the *E. coli* RNR radical-transfer pathway (54, 55), and engineered to study multistep electron tunneling in *Pseudomonas aeruginosa* azurin (56).

Supplementary Material

Refer to Web version on PubMed Central for supplementary material.

Acknowledgments

This work was supported by NIH grants GM079190 (C.T.) and by GM29595 (J.S).

Abbreviations

α2 and β2	subunits of *E. coli* RNR
α_3Y	α_3W and α_3C, *de novo* protein containing a single buried tyrosine, tryptophan or cysteine
α_3X	generic designation for this protein family
α_3(3,5)F_2Y	α_3Y containing 3,5-difluorotyrosine
APB buffer	sodium acetate, potassium phosphate, sodium borate buffer

ATP	adenosine 5′-triphosphate
CDP	cytidine 5′-diphosphate
$E^{\circ\prime}$	formal reduction potential
E_{peak}	voltammetry peak potential
E_{for}	E_{rev} and E_{net}, peak potential of the forward, reverse and net current in SWV
E_{step}	staircase base potential in SWV
E_{SW}	square-wave amplitude
EPR	electron paramagnetic resonance
ET	electron transfer
f	square-wave frequency
F_nY (n = 2, 3)	di- and tri-substituted fluorotyrosines
F_nY. RS	fluorotyrosine aminoacyl-tRNA synthetase
pK_{app}	apparent pK_a
I_{for}	I_{rev} and I_{net}, forward, reverse and net current in SWV
PCET	proton-coupled electron transfer
PGE	pyrolytic graphite edge
RNR	ribonucleotide reductase
SWV	square-wave voltammetry
TPL	tyrosine phenol lyase
Y•	tyrosine radical

REFERENCES

1. Stubbe J, van der Donk WA. Protein radicals in enzyme catalysis. Chem. Rev. 1998; 98:705–762. [PubMed: 11848913]
2. Tommos C, Babcock GT. Proton and hydrogen currents in photosynthetic water oxidation, Biochim. Biophys. Acta. 2000; 1458:199–219.
3. Pesavento RP, van der Donk WA. Tyrosyl radical cofactors. Adv. Protein Chem. 2001; 58:317–385. [PubMed: 11665491]
4. Hoganson CW, Tommos C. The function and characteristics of tyrosyl radical cofactors. Biochim. Biophys. Acta. 2004; 1655:116–122. [PubMed: 15100023]
5. Warren JJ, Winkler JR, Gray HB. Redox properties of tyrosine and related molecules. FEBS Lett. 2012; 586:596–602. [PubMed: 22210190]
6. Harriman A. Further comments on the redox potentials of tryptophan and tyrosine. J. Phys. Chem. 1987; 91:6102–6104.
7. DeFelippis MR, Murthy CP, Faraggi M, Klapper MH. Pulse radiolytic measurement of redox potentials: The tyrosine and tryptophan radicals. Biochemistry. 1989; 28:4847–4853. [PubMed: 2765513]

8. Lind J, Shen X, Eriksen TE, Merényi G. The one-electron reduction potential of 4-substituted phenoxyl radicals in water. J. Am. Chem. Soc. 1990; 112:479–482.
9. DeFelippis MR, Murthy CP, Broitman F, Weinraub D, Faraggi M, Klapper MH. Electrochemical properties of tyrosine phenoxy and tryptophan indolyl radicals in peptides and amino acid analogues. J. Phys. Chem. 1991; 95:3416–3419.
10. Tommos C, Skalicky JJ, Pilloud DL, Wand AJ, Dutton PL. De novo proteins as models of radical enzymes. Biochemistry. 1999; 38:9495–9507. [PubMed: 10413527]
11. Seyedsayamdost MR, Reece SY, Nocera DG, Stubbe J. Mono-, di-, tri-, and tetra-substituted fluorotyrosines: New probes for enzymes that use tyrosyl radicals in catalysis. J. Am. Chem. Soc. 2006; 128:1569–1579. [PubMed: 16448128]
12. Gross AJ, Sizer IW. The oxidation of tyramine, tyrosine, and related compounds by peroxide. J. Biol. Chem. 1959; 234:1611–1614. [PubMed: 13654426]
13. Lehrer SS, Fasman GD. Ultraviolet irradiation effects in poly-L-tyrosine and model compounds. Identification of bityrosine as a photoproduct. Biochemistry. 1967; 6:757–767. [PubMed: 6025562]
14. Boguta G, Dancewicz AM. Radiation-induced dimerization of tyrosine and glycyltyrosine in aqueous solutions. Int. J. Radiat. Biol. 1981; 39:163–174.
15. Karam LR, Dizdaroglu M, Simic MG. OH radical-induced products of tyrosine peptides. Int. J. Radiat. Biol. 1984; 46:715–724.
16. Hawkins CL, Davies MJ. Generation and propagation of radical reactions on proteins. Biochim. Biophys. Acta. 2001; 1504:93–109.
17. Bard, AJ.; Faulkner, LR. Electrochemical methods: Fundamentals and applications. 2nd Ed.. John Wiley & Sons, Inc.; USA: 2001.
18. Savéant, JM. Elements of molecular and biomolecular electrochemistry: An electrochemical approach to electron transfer chemistry. John Wiley & Sons, Inc.; USA: 2006.
19. Warshel A, Sharma PK, Kato M, Xiang Y, Hanbin Liu, Olsson MHM. Electrostatic basis for enzyme catalysis. Chem. Rev. 2006; 106:3210–3235. [PubMed: 16895325]
20. Chandler D. Interfaces and the driving force of hydrophobic assembly. Nature. 2005; 437:640–647. [PubMed: 16193038]
21. Westerlund K, Berry BW, Privett HK, Tommos C. Exploring amino-acid radical chemistry: protein engineering and de novo design. Biochim. Biophys. Acta. 2005; 1707:103–116. [PubMed: 15721609]
22. Martínez-Rivera MC, Berry BW, Valentine KG, Westerlund K, Hay S, Tommos C. Electrochemical and structural properties of a protein system designed to generate tyrosine Pourbaix diagrams. J. Am. Chem. Soc. 2011; 133:17786–17795. [PubMed: 22011192]
23. Berry BW, Martínez-Rivera MC, Tommos C. Reversible voltammograms and a Pourbaix diagram for a protein tyrosine radical. Proc. Nat. Acad. Sci. U.S.A. 2012; 109:9739–9743.
24. Tommos C, Valentine KG, Martínez-Rivera MC, Liang L, Moorman VR. Reversible phenol oxidation and reduction in the structurally well-defined 2-mercaptophenol-α_3C protein. Biochemistry. 2013; 52:1409–1418. [PubMed: 23373469]
25. Dai Q-H, Tommos C, Fuentes EJ, Blomberg MRA, Dutton PL, Wand AJ. Structure of a de novo designed model protein of radical enzymes. J. Am. Chem. Soc. 2002; 124:10952–10953. [PubMed: 12224922]
26. Hay S, Westerlund K, Tommos C. Moving a phenol hydroxyl group from the surface to the interior of a protein: Effects on the phenol potential and pK_A. Biochemistry. 2005; 44:11891–11902. [PubMed: 16128591]
27. Hay S, Westerlund K, Tommos C. Redox characteristics of a de novo quinone protein. J. Phys. Chem. B. 2007; 111:3488–3495. [PubMed: 17388486]
28. Minnihan EC, Young DD, Schultz PG, Stubbe J. Incorporation of fluorotyrosines into ribonucleotide reductase using an evolved, polyspecific aminoacyl-tRNA synthetase. J. Am. Chem. Soc. 2011; 133:15942–15945. [PubMed: 21913683]
29. Osteryoung, J.; O'Dea, JJ. Square-wave voltammetry.. In: Bard, AJ., editor. Electroanalytical chemistry. Vol. 5. Marcel Dekker; New York: 1986. p. 209-308.

30. Mirčeski, V.; Komorsky-Lovrić, Š.; Lovrić, M. Square-wave voltammetry: Theory and applications.. In: F, Scholz, editor. Monographs in electrochemistry. Springer-Verlag; Berlin, Germany: 2007.
31. Minnihan EC, Nocera DG, Stubbe J. Reversible, long-range radical transfer in E. coli class 1a ribonucleotide reductase. Acc. Chem. Res. 2013 10.1021/ar4000407.
32. Yokoyama K, Smith AA, Corzilius B, Griffin RG, Stubbe J. Equilibration of tyrosyl radicals ($Y_{356}^{\bullet}$, $Y_{731}^{\bullet}$, $Y_{730}^{\bullet}$) in the radical propagation pathway of the Escherichia coli Class 1a ribonucleotide reductase. J. Am. Chem. Soc. 2011; 133:18420–18432. [PubMed: 21967342]
33. Chen H, Gollnick P, Phillips RS. Site-directed mutagenesis of His343 → Ala in Citrobacter freundii tyrosine phenol-lyase: Effects on the kinetic mechanism and rate-determining step. Eur. J. Biochem. 1995; 229:540–549. [PubMed: 7744078]
34. Seyedsayamdost MR, Yee CS, Stubbe J. Site-specific incorporation of fluorotyrosines into the R2 subunit of E. coli ribonucleotide reductase by expressed protein ligation. Nat. Protoc. 2007; 2:1225–1235. [PubMed: 17546018]
35. Kim K, Cole PA. Kinetic analysis of a protein tyrosine kinase reaction transition state in the forward and reverse directions. J. Am. Chem. Soc. 1998; 120:6851–6858.
36. Edelhoch H. Spectroscopic determination of tryptophan and tyrosine in proteins. Biochemistry. 1967; 6:1948–1954. [PubMed: 6049437]
37. Pace CN, Vajdos F, Fee L, Grimsley G, Gray T. How to measure and predict the molar absorption coefficient of a protein. Prot. Sci. 1995; 4:2411–2423.
38. Santoro MM, Bolen DW. Unfolding free energy changes determined by the linear extrapolation method. 1. Unfolding of phenylmethanesulfonyl α-chymotrypsin using different denaturants. Biochemistry. 1988; 27:8063–8068. [PubMed: 3233195]
39. Salwiczek M, Nyakatura EK, Gerling UIM, Ye S, Koksch B. Fluorinated amino acids: compatibility with native protein structures and effects on protein–protein interactions. Chem. Soc. Rev. 2012; 41:2135–2171. [PubMed: 22130572]
40. Buer BC, Marsh ENG. Fluorine: A new element in protein design. Prot. Sci. 2012; 21:453–462.
41. Feitelson J, Hayon E. Electron ejection and electron capture by phenolic compounds. J. Phys. Chem. 1973; 77:10–15.
42. Rusling JF. Enzyme bioelectrochemistry in cast biomembrane-like films. Acc. Chem. Res. 1998; 31:363–369.
43. Armstrong FA, Wilson GS. Recent developments in faradaic bioelectrochemistry. Electrochim. Acta. 2000; 45:2623–2645.
44. Armstrong FA. Recent developments in dynamic electrochemical studies of adsorbed enzymes and their active sites. Curr. Opin. Chem. Biol. 2005; 9:110–117. [PubMed: 15811794]
45. Rappaport F, Boussac A, Force DA, Peloquin J, Brynda M, Sugiura M, Un S, Britt RD, Diner BA. Probing the coupling between proton and electron transfer in photosystem II core complexes containing a 3-fluorotyrosine. J. Am. Chem. Soc. 2009; 131:4425–4433. [PubMed: 19265377]
46. Warren JJ, Herrera N, Hill MG, Winkler JR, Gray HB. Electron flow through nitrotyrosine in Pseudomonas aeruginosa azurin. J. Am. Chem. Soc. 2013; 135:11151–11158. [PubMed: 23859602]
47. Dixon WT, Murphy D. Determination of the acidity constants of some phenol radical cations by means of electron spin resonance. J. Chem. Soc. Faraday. Trans. II. 1976; 72:1221–1230.
48. Yokoyama K, Uhlin U, Stubbe J. A hot oxidant, 3-NO_2Y_{122} radical, unmasks conformational gating in ribonucleotide reductase. J. Am. Chem. Soc. 2010; 132:15368–15379. [PubMed: 20929229]
49. Seyedsayamdost MR, Xie J, Chan CTY, Schultz PG, Stubbe J. Site-specific insertion of 3-aminotyrosine in subunit α2 of E. coli ribonucleotide reductase: Direct evidence for involvement of Y_{730} and Y_{731} in radical propagation. J. Am. Chem. Soc. 2007; 129:15060–15071. [PubMed: 17990884]
50. Seyedsayamdost MR, Stubbe J. Site-specific replacement of Y_{356} with 3,4-dihydroxyphenlalanine in the β2 subunit of E. coli ribonucleotide reductase. J. Am. Chem. Soc. 2006; 128:2522–2523. [PubMed: 16492021]

51. Tsai A-L, Kulmacz RJ. Prostaglandine H synthesis: Resolved and unresolved mechanistic issues. Arch. Biochem. Biophys. 2010; 493:103–124. [PubMed: 19728984]

52. Aubert C, Vos MH, Mathis P, Eker APM, Brettel K. Intraprotein radical transfer during photoactivation of DNA photolyase. Nature. 2000; 405:586–590. [PubMed: 10850720]

53. Tarboush NA, Jensen LMR, Yukl ET, Geng J, Liu A, Wilmot CM, Davidson VL. Mutagenesis of tryptophan 199 suggests that hopping is required for MauG-dependent tryptophan tryptophylquinone biosynthesis. Proc. Nat. Acad. Sci. U.S.A. 2011; 108:16956–16961.

54. Uhlin U, Eklund H. Structure of ribonucleotide reductase protein R1. Nature. 1994; 370:533–539. [PubMed: 8052308]

55. Ekberg M, Birgander P, Sjöberg B-M. In vivo assay for low-activity mutant forms of Escherichia coli ribonucleotide reductase. J. Bacteriol. 2003; 185:1167–1173. [PubMed: 12562785]

56. Shih C, Museth AK, Abrahamsson M, Blanco-Rodriguez AM, Di Bilio AJ, Sudhamsu J, Crane BR, Ronayne KL, Towrie M, Vlcek A Jr. Richards JH, Winkler JR, Gray HB. Tryptophan-accelerated electron flow through proteins. Science. 2008; 320:1760–1762. [PubMed: 18583608]

GSR(1)–**VKALEEKVKALEEKVKA**–*LGGGGR*–**IEELKKKX(32)EELKKKIEE**–*LGGGGE*–**VKKVEEEVKKLEEEIKK**–*L(65)*

Scheme 1.

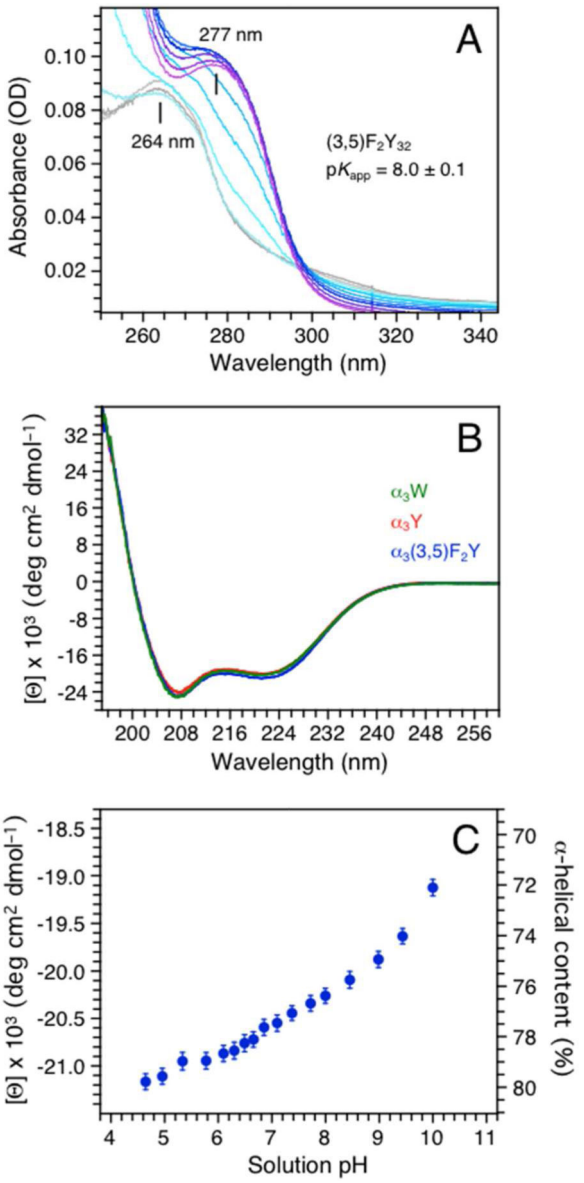

Figure 1.

(**A**) A pH titration of $\alpha_3(3,5)F_2Y$ monitored by UV-Vis absorption spectroscopy. Spectra were collected at pH 5.72 (gray), 6.38, 6.84, 7.49, 8.06, 8.53, 8.96, 9.31, 9.59, 10.02 and 10.42 (purple). (**B**) Far-UV CD spectra of $\alpha_3(3,5)F_2Y$ (blue), α_3Y (red) and α_3W (green) in 20 mM sodium acetate, pH 5.62 ± 0.01. The single aromatic residue in each protein is fully protonated at this pH. The CD spectra are displayed in units of mean residue molar ellipticity ([Θ]) obtained by: $([\Theta]) = \theta_{obs}(10^6/CIn)$ where θ_{obs} is the observed ellipticity in mdegrees (spectrometer raw signal), C the protein concentration in μM, l the cuvette path length in mm, and n the number of amino-acid residues (65). $[\Theta]_{222}$ equals $-20.0 \pm 0.8 \times 10^3$ deg cm^2 dmol^{-1} at pH 5.6 for $\alpha_3(3,5)F_2Y$ (Table 1). (**C**) Changes in the mean residue molar ellipticity ([Θ]) and the corresponding % α-helical content of $\alpha_3(3,5)F_2Y$ between pH 4.7 and 10.

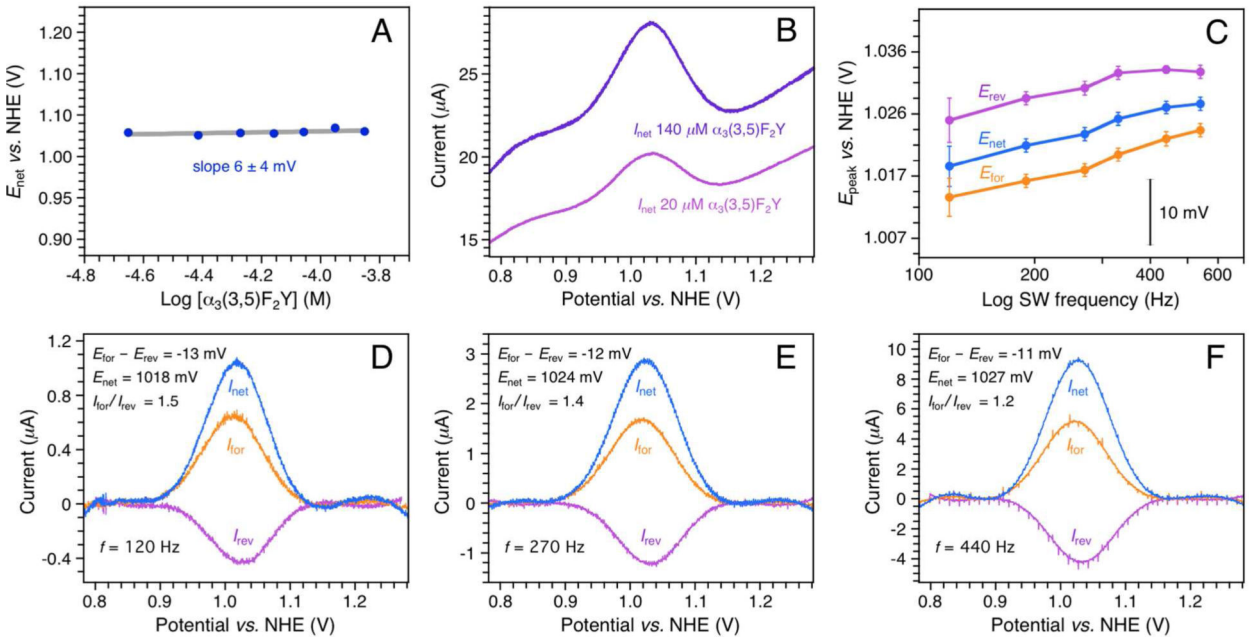

Figure 2.

SWV analysis of the Y-O•/Y-OH redox system in $\alpha_3(3,5)F_2Y$. (**A**) E_{net}(270 Hz) as a function of [$\alpha_3(3,5)F_2Y$], pH 5.53 ± 0.11. E_{net} is independent of the protein concentration, which is consistent with benign protein/working electrode interactions. (**B**) Representative net voltammograms (I_{net}) collected at the upper (140 μM, purple) and lower (20 μM, magenta) limit of the [$\alpha_3(3,5)F_2Y$] data series shown in panel A. The Faradaic response is optimal in this protein concentration range. (**C**) Peak potential of the forward (E_{for}), reverse (E_{rev}) and net (E_{net}) $\alpha_3(3,5)F_2Y$ voltammograms as a function of the SW frequency (*f*), pH 5.70 ± 0.02. (**D**, **E** and **F**) Background-corrected voltammograms from the data series shown in panel C. SWV settings: 20 mM APB, 75 mM KCl, PGE working electrode, temperature 25° C, step potential 0.15 mV, SW pulse amplitude 25 mV.

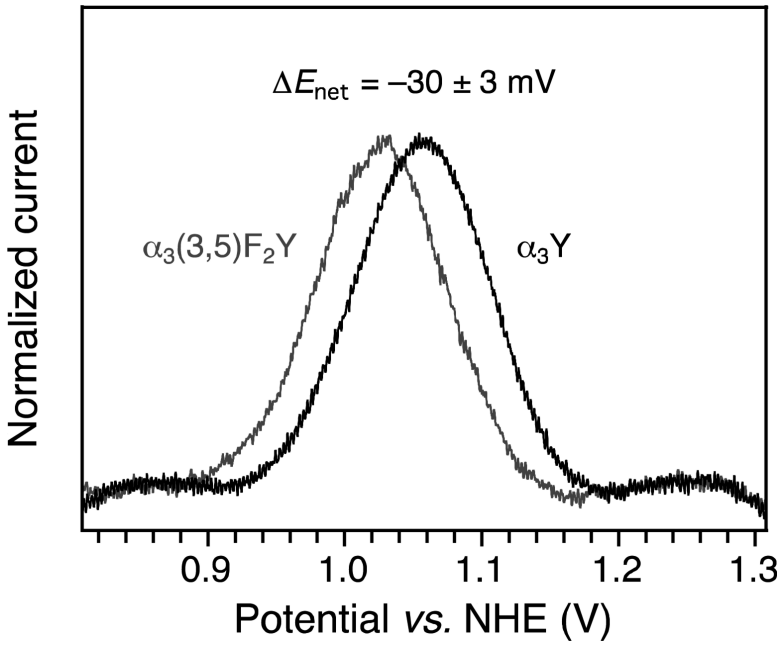

Figure 3.

I_{net} of $\alpha_3(3,5)F_2Y$ (grey) and α_3Y (black) recorded at identical experimental conditions. SWV settings: 20 mM APB, 75 mM KCl, pH 5.62 ± 0.02, PGE working electrode, temperature 25° C, step potential 0.15 mV, SW frequency 190 Hz, SW pulse amplitude 25 mV.

Table 1

Properties of Y, 3,5-F_2Y, α_3Y and α_3(3,5)F_2Y

System	λ_{max} (nm) / ε (M^{-1} cm^{-1})	pK_a [pK_{app}]	Potential *vs.* NHE (mV)[e]	Ref.
Y(Ac/NH_2)[a]	275/1400 (Y-OH) 293/2420 (Y-O-)	10	E_{peak} 830 (pH 7.0)	31
3,5-F_2Y(Ac/NH_2)[a]	263/560 (Y-OH) 275/1830 (Y-O-)	7.0 ± 0.2	E_{peak} 770 (pH 7.0)	31
α_3Y	277/1500 (Y-OH, pH 5.4) 294/2430 (Y-O-, pH 13.4)	[11.3 ± 0.1]	$E^{\circ\prime}$ 1059 (pH 5.7) $E^{\circ\prime}$ 980 (pH 7.0)	10, 22, 23 this work
α_3(3,5)F2Y	~264/n.d. (Y-OH)[a] ~277/n.d. (Y-O-)[a]	[8.0 ± 0.1]	$E^{\circ\prime}$ 1026 (pH 5.7) $E^{\circ\prime}$ 952 (pH 7.0)[f]	this work

System	$[\Theta]_{222} \times 10^3$ (deg cm^2 $dmol^{-1}$)	Helix (%)[b]	ΔG (kcal mol^{-1})[g]	Ref.
α_3Y	−20.0 ± 0.8 (pH 5.6)	75 ± 3 (pH 5.6)[c] 74 ± 1 (4.5-10)[d]	−3.7 ± 0.1 (pH 5.0) −3.9 ± 0.1 (pH 5.5)	10, 22, this work
α_3(3,5)F_2Y	−20.9 ± 0.6 (pH 5.6)	79 ± 2 (pH 5.6)[c]	−3.7 ± 0.1 (pH 5.0) −3.7 ± 0.1 (pH 5.5)	this work

[a] Acetyl-tyrosinamide (Ac/NH_2), ε was not determined (n.d.).

[b] Scaled relative to the $[\Theta]_{222}$ of α_3W (76 ± 1% α-helical, pH 4-10; 10, 25).

[c] [Protein] determined by the Bradford assay.

[d] [Protein] determined by UV absorption (10, 22).

[e] Anodic peak potentials from irreversible differential pulse voltammograms (E_{peak}; 10, 11, 31). The standard error in $E^{\circ\prime}$ is ± ± 4 mV.

[f] Extrapolated from the pH 5.7 value and assuming the same pH dependence as observed for α_3Y $E^{\circ\prime}$(pH 5.7) and $E^{\circ\prime}$(pH 7.0)(23).

[g] From Fig. S5.